Original research article

Targeted Therapy in Liver Tumor: Study on Nanoparticle Assisted with Porous Liver Model

Suchai Pongpakpien, Niti Shaichompu, Phadungsak Rattanadecho[*]

Department of Mechanical Engineering, Faculty of Engineering, Thammasat University, Pathum Thani 12120, Thailand

ABSTRACT

The high performance of Microwave ablation (MWA) is measured by the successful coagulate of the target tissues with less effect on the surrounding healthy tissues. To achieve this goal, the precious porous liver model is used for simulation to investigate how the performance improves when two key properties, thermal and electrical conductivity, have been changed. The investigation of selected nanoparticle, Carbon Nanotube (CNT), also has been included. The result has shown that increased thermal and electrical conductivity of target tissue in the porous liver promotes a higher heating rate and lower maximum temperature when compared with the normal porous liver tissue condition. The MWA performance improved when the selected nanoparticle CNT was included, producing an improved lesion shape with a short tail when compared with normal tissues. In summary, this study gives the necessary aspect for knowledge of enhancing the MWA process and can be used as a guideline to enhance the MWA efficacy.

Keywords: Porous liver model; Microwave ablation; Nano assisted; Thermal conductivity; Electrical conductivity

1. Introduction

Targeted therapy, especially MWA, is a highly effective method due to the good result of demolishing unhealthy target tissue [1-2]. The advantage of MWA, compared to other energy sources, for example, laser, radiofrequency, or ultrasound, is the larger ablating zone and depth effectiveness [3-9].

Several MWA improvements have been presented in recent years. Many antenna designs have been presented, such as cooled-shaft antenna [10-11], Tri-axial [12-13], floating sleeve [14-15], and slot antenna [16-17]. The most suitable is the slot antenna because of the comfortable size and high effective coagulating result

*Corresponding author: ratphadu@engr.tu.ac.th

[18-19]. The key factors during the ablation process, duration and input microwave power, have been studied by Keangin et al. [20]. However, there remains a limitation of MWA since, even with recent improvement strategies, the slot antenna gives the lesion backward heating and damages the surrounding healthy tissues [21-23].

In this study, the porous liver model with the energy equation and momentum equation has proposed. The influence of thermal and electrical conductivity in the porous liver model along with selected nanoparticles, Carbon Nanotube (CNT) has been investigated. The residual tail or backward heating reduces 300 % when the higher thermal conductivity CNT is loaded to targeted tumor. The investigation gives the essential aspect of a fundamental understanding of heat transport within porous liver cancer. The enhancement of MWA with a nanoparticle has been investigated and can be used as a guideline to enhance the efficacy design of MWA.

Nomenclature

k	: propagation constant (m^{-1})
C	: speed of light (m/s)
r	: dielectric radius (m)
$\vec{H}$	: Magnetic field (A/m)
u, w	: velocity component (m/s)
p	: pressure (Pa)
d_p	: diameter of cell tissue (m)
C_p	: specific heat capacity (J/kg °C)
$\vec{E}$	: Electric field (V/m)
g	: gravitation constant (m^2/s)
K	: thermal conductivity (W/(m°C)
P	: input microwave power (W)
Q	: heat source (W/m^3)
t	: time (s)
T	: temperature (°C)

Greek Symbols

ω	: angular frequency (rad/s)
ρ	: density of liver tissue (kg/m^3)
ε_0	: permittivity of free space (F/m)
ε_r	: relative permittivity (-)
σ	: electric conductivity (S/m)
μ	: permeability (H/m)
μ_r	: relative permeability
ν	: kinematics viscosity (m^2/s)
ϕ	: tissue porosity
β	: coeff. of thermal expansion (K^{-1})
κ	: permeability (m^2)

Subscripts

b	: blood/fluid phase
t	: tissue/solid phase
ext	: external
eff	: effective value
inner	: inner
liver	: liver
met	: metabolism

2. Problem Statement
2.1 The backward heating problem

Backward heating remains a serious effect in the MWA process. It has been more serious when input power and operating durations are increased due to larger lesions [20]. Fig. 1 shows the backward heating problem. The photo took by our experiments was performed ex-vivo with bovine liver tissue. This photo clearly shows a tear-drop shape lesion with a long tail.

Fig. 1. Demonstration of backward heating shape.

To leverage the MWA performance, two key tissue properties, thermal conductivity and electrical conductivity, are the main factors for heat transportation in tissue. There are few studies that investigate these factors and how the influence of thermal and electrical conductivity affects the blood velocity and temperature distribution in the ablation zone. The nanoparticle is required to elevate these two

properties and investigate the result of how improving performance on temperature distribution and the ablation zone.

The influences of thermal and electrical conductivity with selected nanoparticles CNT are investigated. The newly investigated nano-hyperthermia proposed interesting ability in tumor treatment [36]. Nano-assisted cryosurgery has been proposed with interesting results [37]. The magnetite (Fe_3O_4), Magnesium Oxide (MgO) and Diamond have been used to promote the thermal ablation [38]. The cylindrical carbon nanotube (CNT) has been introduced to RFA treatment and showed good performance in the absorption of excess radiofrequency radiation [39].

In recent years, the good performance of nanoparticle assisted hyperthermia has shown positive impact [24]. Furthermore, the success of loading nanoparticles into a liver tumor is effective, to leverage the thermal and conductivity properties of liver tumor [25-27]. Unfortunately, only a few existing research studies report the investigation of MWA performance liver tumor therapy with nanoparticle assistance.

2.2 The precision of simulation heat transfer model

The key study in MWA performance is the precious heat transfer model. It is a tool to predict and enhance the MWA treatment process. Unfortunately, there are few studies in the realistic physical model of the liver tumor due to the complexity of the biological tissue which includes liver tissue, cells and microvascular elements. Only a few studies have considered the heat transfer model with porous media theory [28-30].

The porous liver model with the energy equation and momentum equation has been proposed. The influence of thermal and electrical conductivity in the porous liver model along with selected nanoparticles, Carbon Nanotube (CNT) has been investigated. The transient momentum

equation (Brinkman model extended with Darcy model) together with the transient energy equation including the electromagnetic equation, has been conducted. The simulation equation and boundary conditions are calculated by using the axisymmetric FEM via COMSOL™ Multiphysics. The proposed model has been verified with previous bio-heat models and experimental results with the same conditions. The simulation results of temperature distribution, blood velocity profile with influences of thermal and electrical conductivity factor and the selected nanoparticles CNT are presented.

3. Simulation Methodology
3.1 Slot microwave antenna model

The single-slot microwave antenna was used because of the appropriate size for insertion into the human liver. Fig. 2 shows the antenna model structure with a slot ring of 1 mm. and the position of the slot 5.5 mm from the short circuit tip. The operating frequency is 2.45 GHz. Table 1 and Fig. 2 give the antenna dimensions and dielectric properties, respectively [20].
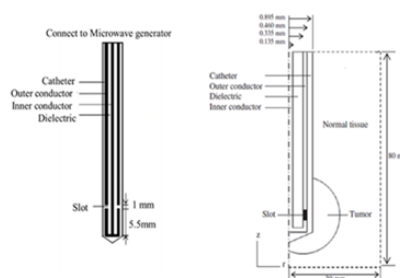

Fig. 2. Structure of the antenna and Axis symmetrical model structure [20].

3.2 Porous liver model

The porous liver can be separated into three main parts which are blood vessels, cells, and interstitial space [29-30]. The porous liver has two distinct regions. One is the vascular region (blood vessels/fluids phase) and the other is the extravascular

region (tissue cell and interstitial space/solid phase). This assumes that the whole anatomical structure is a fluid-saturated porous medium through which the blood infiltrates [30]. The porous liver model in this study is considered into two parts, tumor and normal liver tissue. Fig. 2 shows the porous liver model structure.

Table 1. The dielectric properties of a slot microwave antenna [20].

Properties	Dielectric	Catheter	Slot
Relative permittivity, ε_r (-)	2.03	2.1	1
Electric conductivity, σ (s/m)	0	0	0
Relative permeability, μ_r (-)	1	1	1

Table 2. Properties of tissue, blood and tumor [30-32].

Properties	Normal tissue	Blood	Tumor
Thermal Conduct K (W/m °C)	0.497	0.45	0.57
Density ρ (kg/m³)	1,030	1,058	1,040
Specific heat capacity C_p (J/kg. °C)	3,600	3,960	3,960
Relative Permittivity ε_r	43.00	58.30	48.16
Electric conductivity σ (S/m)	1.69	2.54	2.096

The tumor is a spherical shape with a diameter of 20 mm. The axis-symmetric model is used to minimize the calculation time while maintaining a good resolution. The thermal conductivity properties and dielectric properties of normal tissues and tumors are given in Table 2 [30-32].

3.3 The mathematical model
The electromagnetic field propagation in microwave coaxial antenna and equation for heat transfer with blood flow are described as follows:

3.3.1 Electromagnetic field
The equation of electric field and magnetic fields in the Transverse Electromagnetic field (TEM), which propagate in the coaxial antenna, is described in symmetrical cylindrical coordinates (2D axis r-z):

Electric field
$$\bar{E} = e_r \frac{c}{r} e^{j(\omega t - kz)} \qquad (1)$$

Magnetic field
$$\bar{H} = e_\varphi \frac{c}{rz} e^{j(\omega t - kz)} \qquad (2)$$

where
$$C = \sqrt{\frac{ZP}{\pi \cdot \ln(r_{outer} / r_{inner})}} \qquad (3)$$

The inner dielectric radius (r_{outer}) and the outer dielectric radius (r_{inner}) are given in Fig 2. [20].

In a typical MWA using a slot antenna, the thermal energy is created from the conversion of the magnetic energy when the magnetic field is radiated to the target porous liver. The Transverse Magnetic field is represented by the following equation.

$$\nabla \times \left[\left[\varepsilon_r - \frac{j\sigma}{\omega \varepsilon_0} \right]^{-1} \nabla \times \bar{H}_\varphi \right] - \mu_r k_0^2 \bar{H}_\varphi = 0, (4)$$

where $\varepsilon_0 = 8.8542 \times 10^{-12}$ F/m [11], relative permittivity $(\varepsilon_r) = 2.03$, the electric conductivity $(\sigma) = 0$ and relative permeability $(\mu_r) = 1$.

Meanwhile, the boundary conditions for axis symmetry at $r = 0$, boundary condition for porous liver and slot antenna boundary condition and electromagnetic wave propagation assumption have been obtained from literature P. Keangin et al [20]. Fig. 3 shows the detail of the boundary condition for this study.

3.3.2 Equation for blood flow and thermal transport
To study the transient temperature distribution within the porous liver tumor and normal tissue as shown in Fig. 3, the coupled model of electromagnetic wave propagation, blood flow, and thermal transport were analyzed. The surrounding of the porous liver is equal to 37 °C as fixed temperature whereas the surface between
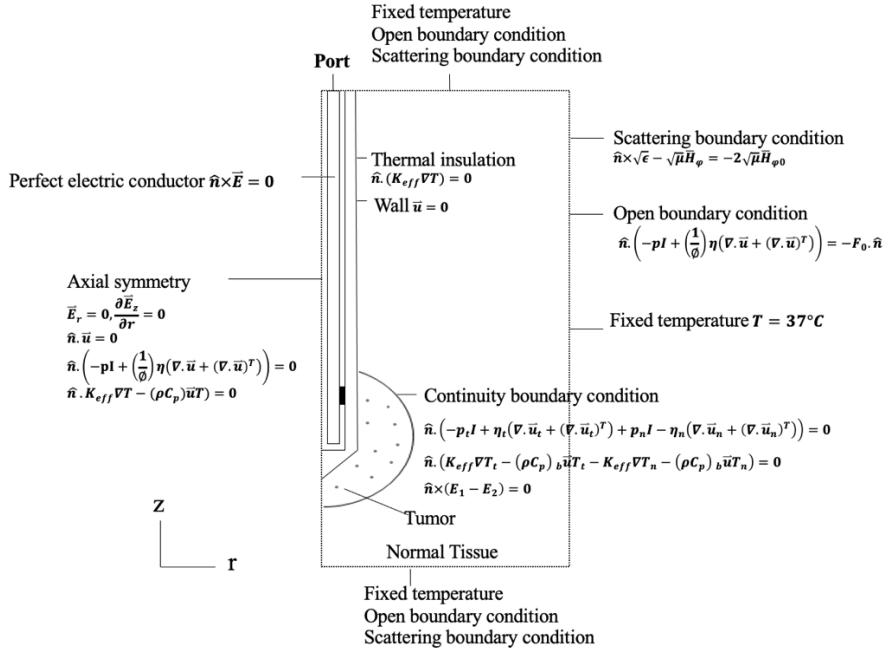
Fig. 3. Boundary conditions for this study.

the antenna and the porous liver, the adiabatic boundary condition has been considered. For simplicity, several assumptions have been obtained from our previous group work [33].

3.3.3 Momentum equation

To describe the blood flow phenomenon in porous liver tumors and normal tissue, the Brinkman model extended Darcy model is used. The equations that explain the blood flow in the porous liver are given from the continuity equation (5) and momentum equation (6) and (7) as follows [33]:

$$\frac{\partial u}{\partial r} + \frac{\partial w}{\partial z} = 0, \tag{5}$$

$$\frac{1}{\phi}\left[\frac{\partial u}{\partial t}\right] + \frac{1}{\phi^2}\left[u\frac{\partial u}{\partial r} + w\frac{\partial u}{\partial z}\right]$$

$$= -\frac{1}{\rho_b}\left[\frac{\partial p}{\partial r}\right] + \frac{v}{\phi}\left[\frac{\partial^2 u}{\partial r^2} + \frac{\partial^2 u}{\partial z^2}\right] - \frac{uv}{\kappa}, \tag{6}$$

$$= \frac{1}{\phi}\left[\frac{\partial w}{\partial t}\right] + \frac{1}{\phi^2}\left[u\frac{\partial w}{\partial r} + w\frac{\partial w}{\partial z}\right]$$

$$= -\frac{1}{\rho_b}\left[\frac{\partial p}{\partial z}\right] + \frac{v}{\phi}\left[\frac{\partial^2 w}{\partial r^2} + \frac{\partial^2 w}{\partial z^2}\right] - \frac{wv}{\kappa} \tag{7}$$

$$+ g\beta(T - T_\infty).$$

The tumor porosity $(\phi_{tumor}) = 0.7$ and normal tissue porosity $(\phi_{n\_tissue}) = 0.6$. The kinematics viscosity $(v) = 3.78\times10^{-7}$ m²/s, the coefficient of thermal expansion $(\beta) = 11\times10^{-4}$ K⁻¹. The permeability (κ) can be calculated by the following equation [33]:

$$\kappa = \frac{\phi^3 d_p^2}{175(1-\phi)^2}, \tag{8}$$

where diameter of cell tissue $(d_p) = 1\times10^{-4}$ m²

3.3.4 Energy equation

The transient energy equation governing the thermal phenomena that is created in porous liver tumor have been described as [33]:

$$\left(\rho C_p\right)_{eff}\frac{\partial T}{\partial t}+\left(\rho C_p\right)_b\left[u\frac{\partial T}{\partial r}+w\frac{\partial T}{\partial z}\right]$$
$$=K_{eff}\left[\frac{\partial^2 T}{\partial r^2}+\frac{\partial^2 T}{\partial z^2}\right]+Q_{met}+Q_{ext}, \tag{9}$$

$$\left(\rho C_p\right)_{eff}=(1-\phi)\left(\rho C_p\right)_t+\phi\left(\rho C_p\right)_b, \tag{10}$$

$$K_{eff}=(1-\phi)K_t+\phi K_b, \tag{11}$$

The external heat source (Q_{ext}) has been created by the electromagnetic and assumes created from tissue/solid phase only, can be expressed as [33]:

$$Q_{ext}=\frac{\sigma\left|\vec{E}\right|^2}{2} \tag{12}$$

3.3.5 The cooperated nanoparticle in MWA calculation

3.3.5.1 Thermal conductivity

The conventional Hamilton-Crosser (H-C) model was used to calculate the cooperated thermal conductivity between nanoparticle and liver tumor tissue [34]. When the spherical nanoparticle is injected into the space between cells, the H-C model expresses the merged thermal conductivity and heat capacity as

$$k_{effnp}(T)\cdot\frac{k_{np}+2k_{eff}(T)+2\eta(k_{eff}(T)-k_{np})}{k_{np}+2k_{eff}(T)-\eta(k_{eff}(T)-k_{np})}, \tag{13}$$

$$C_{effnp}(T)\rho_{effnp}=C_{eff}(T)\rho_{eff}(1-\eta)+C_{np}\rho_{np}\eta, \tag{14}$$

For the non-spherical structure merged nanoparticle CNT calculation. Glory et al [35] have proposed thermal conductivity for non-spherical nanoparticle as the following equation:

$$k_{effnp}(T)=k_{eff}(T)\cdot\frac{k_{eff}+(n-1)k_{np}-(n-1)\eta(k_{eff}(T)-k_{np})}{k_{eff}+(n-1)k_{np}-\eta(k_{eff}(T)-k_{np})}, \tag{15}$$

where $n=\left(\frac{12L}{d}\right)^{1/3}$. $\tag{16}$

3.3.5.2 Electrical conductivity

In this study the electrical conductivity model of nanoparticle was applied from the Maxwell model [31]. The effective electrical conductivity when merged with nanoparticle is expressed by the following equation:

$$\rho_{effnp}(T)=\rho(T)\cdot\frac{3(\rho_{np}(T)-\rho(T))\eta}{(\rho_{np}(T)+2\times\rho(T))-(\rho_{np}(T)-\rho(T))\eta}, \tag{17}$$

Since the nanoparticle has much larger conductivity than the liver tumor, the equation (17) can rewrite as

$$\sigma_{effnp}=(1+3\eta)\sigma. \tag{18}$$

3.4 Calculation procedure

The transient phenomenon has been analyzed by using the Finite Element Method (FEM) based on COMSOL™ multiphysics. Two models of an electromagnetic equation with blood flow equation and heat transport are constructed. The temperature distribution, blood flow and ablation area that occur in the porous liver are described. The simulation starts from calculating the electromagnetic wave which creates heat sources in terms of an external heat source. Then it calculates the time-dependent temperature that occurs in the porous liver. The calculation process continues until the target heating time is reached. The axisymmetric FEM model is uses the triangular element with Lagrange quadratic shape functions. The partial differential equations with the designed boundary are conducted. The simulation was conducted until the stability results in which the independent fine mesh is to be around 22,405.

4. Result and Discussion
4.1. The model verification

The verification of the present porous liver model is compared with the simulation result of Keangin et al. [20] and experimental result of Yang et al. [31]. All conditions were set in the same way; input microwave power was 75 W with frequency 2.45 GHz with the temperature starting from 8 °C and the antenna insertion depth was 20 mm. The validation results are shown in Fig. 4 for the temperature distribution in the porous liver tissue at positions 4.5 mm. and 9.5 mm. away from the slot antenna. The result shows that the porous model complies better with the experimental data than the conventional bioheat at the same approximate time range. The porous liver shows performance with convective heat together with conduction heat, while the conventional bioheat is contained with only conduction heat mode.

The porous liver model has been studied for prediction when the key properties in the model have been changed. The influence of two key properties, the thermal conductivity (K) and electrical conductivity (σ), on the temperature distribution in the porous liver with blood flow has been investigated. The tumor is the spherical shape with a diameter of 10 mm. A study of each parameter has been conducted to investigate the result of each factor separately. The results of changed properties when nanoparticles are applied to cells also have been investigated.

4.2 The influence of thermal and electrical conductivity in porous liver with blood flow model

The effective performance of MWA depends on the characteristics of the temperature profile, which determines the key property thermal conductivity in the MWA process. The simulation of various thermal conductivity properties in the porous liver has been conducted. The heating time is 300 sec. and microwave input power (P) is 10 watts. Fig. 5 (a) - 5 (d) show the temperature profile and blood flow profile within the porous liver. The various thermal conductivities of tumors have been investigated by increasing 1.5, 2.0, and 4.0 times of the normal tumor condition respectively. The figure illustrates the hot spot zone, maximum temperature and blood velocity for each condition.

The effectiveness of the MWA process is to elevate the precision of the ablation area without affecting the healthy tissue around the tumor. In this section, the effects of thermal property in the ablation zone in the porous liver with blood flow model have been investigated. Fig. 6 shows the geometry of the temperature measurement points along with the arc of the tumor. The microwave input power is 10 watts. Fig. 6 (a) – 6(d) shows the result of temperature at each measurement point within the various thermal properties. It is found that when the thermal conductivity increases, the maximum temperature will decrease. Furthermore, an increase in thermal conductivity such as 100 or 1000 times, results in a smaller variation of temperature in the porous liver. This is because increased thermal conductivity will generate heat to all areas rapidly with blood flow and makes temperature distribute in a uniform shape.

4.3 The influence of selected nanoparticles on thermal and electrical conductivity in porous liver

The nanoparticle CNT with volume fraction $\eta = 0.5$ was loaded in the equation 13 to 18, and the result compared with normal tumor tissue condition. Fig. 7 shows the simulation result of the tumor temperature contour between normal tissue and loaded nanoparticle CNT with volume fraction $\eta = 0.5$. The red line is the 50 °C line. Fig. 7 (a) shows the red line that did not cover the tumor 100% even though the simulation duration reaches 1000 sec. and produces a 12 mm. tail range. Fig. 7(b)
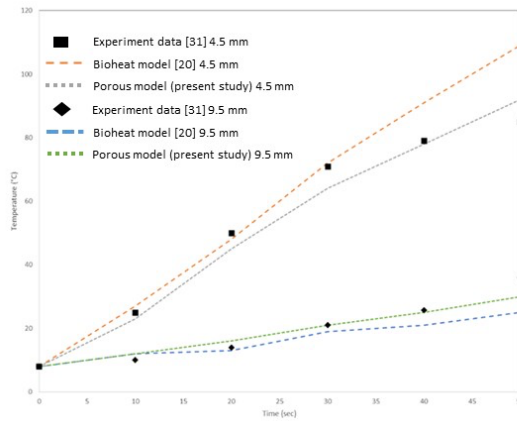
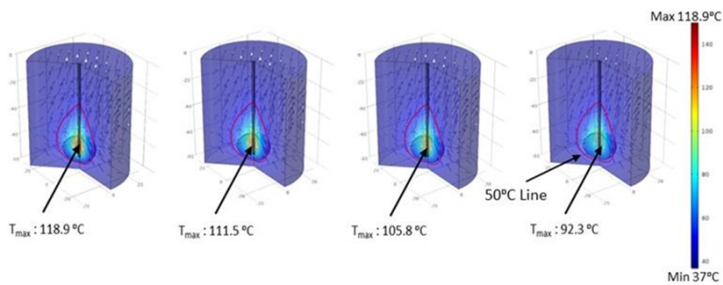**Fig. 4.** The Verification result of the liver tissue temperature.

Fig. 5. The temperature pattern and blood flow vector within the porous liver at various thermal conductivity: (a) Normal tumor thermal conductivity (b) Increase 1.5 time of normal tumor condition (c) Increase 2 time of normal tumor condition (d) Increase 4 time of normal tumor condition.
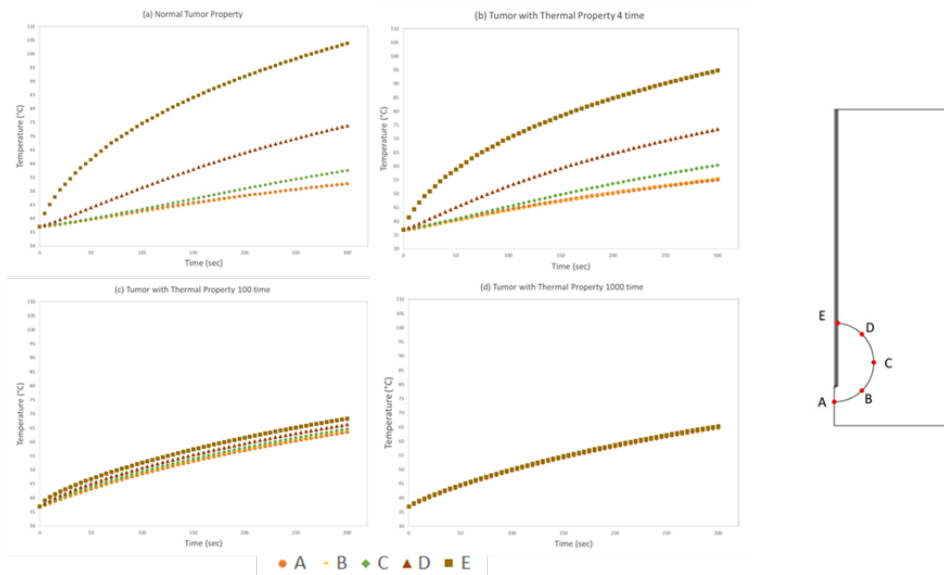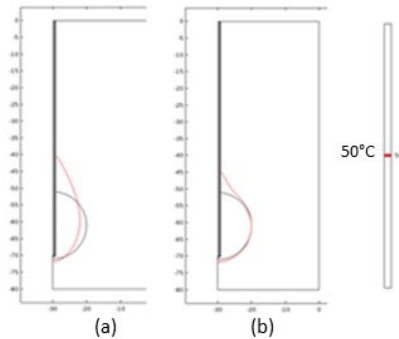

Fig. 6. The temperature distribution along the arc section of tumor at various porous liver thermal conductivity properties: (a) Normal tumor thermal conductivity (b) Increase 4 time of normal tumor condition (c) Increase 100 time of normal tumor condition (d) Increase 1000 time of normal tumor condition.

shows the red line covers the tumor 100% with a simulation time 75 sec. and produces a 4 mm. tail range. Since the CNT has increased the thermal conductivity in tumor tissue, the improved performance of MWA can be concluded from these comparisons.

Fig. 7. Temperature contour compare between (a) Normal tissue and (b) nanoparticle CNT loaded with volume fraction $\eta = 0.5$.

5. Conclusion

The Microwave ablation mathematical simulation model of heat transfer and blood flow within the porous liver has been developed. Specifically, we studied the influence of thermal and electrical properties on treatment outcome and efficacy. The mathematical model has been validated with the experimental data from a previous work [31]. It was found that the simulation result of the porous liver model has better results than a conventional bioheat model when compared with previous experimental data [31].

Clinical treatment with MWA requires accurate control of various parameters due to the need for lesion creation without effect to healthy tissue. To enhance the MWA process, the proposed porous liver tumor with two key properties has been investigated. Two key properties, thermal conductivity and electrical conductivity, were selected and studied in more detail for the effectiveness in the improvement MWA process. The selected nanoparticle CNT has been included and studied by using the conventional Hamilton-Crosser (H-C) thermal conductivity model

[34]. The two main properties in the porous liver model have been recalculated on the volume fraction. The thermal and electrical effects of sharing by volume fraction between selected nanoparticle and liver tumor properties, using the porous liver model were examined. The simulation was conducted and key findings that emerged from the result include:

(1) The proposed porous liver model gave better results than conventional bioheat when compared to the previous experimental data. It can be confirmed that the porous media theory is the most suitable theory for heat transfer in biological tissue. The proposed porous liver model with momentum equation is proven and can be applied to the realistic model in the MWA process simulation.

(2) The higher thermal conductivity is introduced to the targeted tumor tissue and it was found that the maximum temperature is reduced due to the heat transfer and blood flow even though the temperature was still higher than 50°C in the ablating zone. To promote heat transfer between MWA antenna and target tumor tissue, some particles having high thermal conductivity properties such as nanoparticle needed to be introduced and investigated in the future study. For the same situation, when higher electrical conductivity is introduced to the targeted tumor tissue, the maximum temperature, and heating rate are increased.

(3) The higher thermal conductivity promotes the MWA treatment by lowering the hot spot zone of tumor tissue temperature, leading to a more uniform temperature distribution within the tumor tissue. The higher thermal conductivity gives lower variation temperature in the targeted tumor. This is very useful for elevating MWA efficiency and decreasing harmful effects during the MWA process.

(4) The residual tail or backward heating reduces 300 % when the higher thermal conductivity CNT is loaded to targeted tumor since high thermal

conductivity causes the temperature distribution to be uniform and absorb the temperature created from microwave power better than no particle loaded tumor tissue.

This key investigation obtained the necessary aspects of knowledge for enhancing the MWA treatment process. It can be used as a guideline to further study in enhancing the MWA treatment process. Even though backward heating remains, the technique gives better results and improves the MWA process treatment.

Acknowledgements

References

[1]   C.J. Simon, D.E. Duuy. And W.W. Mayo-smith (2005). Microwave ablation: principles and application, Radiographics, vol. 25, October 2005, pp. S69-83.

[2]   Alan A.S. Amad, Abimael F.D. Loula, Antonio A. Novotny (2017). A new method for topology design of electromagnetic antennas in hyperthermia therapy, Applied Mathematical Modelling, vol. 42, pp. 209-22.

[3]   J.C. Lin, P. Bernardi, S. Pisa, M. Cavagnaro and E. Piuzzi (2008). Antenna for medical theraphy and diagnotics. Modern Antenna Handbook, C. Balanis, Ed., Newyork: Wiley. pp. 1377-428.

[4]   A. Karampatzakis, S. Khun, G. Tsanidis, E. Neufeld, T. Samaras and Niels Kuster (2013). Heating characteristics of antenna arrays used in microwave ablation: A theoretical parametric study, Computers in Biology and Medicine, vol. 43 pp. 1321-7.

[5]   T.L. Wonnel, P.R. Stauffer and J.J. Langberg (1992). Evaluation of

microwave and radio frequency catheter ablation in a myocardium-equivalent phantom model, IEEE Trans. Biomed. Eng., vol. 39 (10) pp. 1086-95.

[6]   J.C. Lin, Y.L. Wang and R.J. Heriman (1994). Comparison of power deposition pattern produced by microwave and radio frequency cardiac ablation catheters, Electron. Lett., vol. 30(12), pp. 922-3.

[7]   D.L. Deardorff, C.J. Diederich and W.H. Nau (2001). Control of interstitial thermal coagulation: Comparative evaluation of microwave and ultrasound applicator, Med. Phys. Vol. 28(1), Jan. 2001, pp. 104-17.

[8]   M.M. Attar, M. Haghpanahi, S. Amanpour and M. Mohaqeq (2014). Analysis of bioheat equation for hyperthermia cancer treatment, Journal of mechanical Science and Tech., vol. 28(2), 2014, pp. 763-71.

[9]   A.S. Wright, L.A. Sampson, T.F. Warner, D.M. Mahvi, and F.T. Lee Jr. (2005). Radiofrequency versus microwave ablation in a hepatic porcine model, radiology, vol. 236 pp. 132-9.

[10]   D. Jiao, L. Qian, Y. Zhang, F. Zhang, C. Li, Z. Huang, L. Zhang, W. Zhang, P. Wu, X. Han, G. Duan and J. Han (2010). Microwave ablation treatment of liver cancer with 2,450 MHz cooled-shaft antenna: an experimental and clinical study, Journal of Cancer Research and Clinical Oncology, vol. 136 (10), October 2010, pp. 1507-16.

[11]   Y. Sun, Z. Cheng, L. Dong, G. Zhang, Y. Wang and P. Liang (2012). Comparison of temperature curve and ablation zone between 915 and 2450 MHz cooled shaft microwave antenna: result in ex vivo porcine livers, European Journal of Radiology, vol. 81 (3), March 2012, pp. 553-7.

[12]   C.L. Brace, D.W. Van Der Weide, F.T. Lee Jr., P.F. Laeseke and L. Sampson (2004). Analysis and experimental

validation of a triaxial antenna for microwave tumor ablation, IEEE MTT-S International Microwave Symposium Digest, vol. 3 (6-11), January 2004, pp. 1437-40.

[13] C.L. Brace, P.F. Laeseke, L.A. Sampson, T.M. Frey, D.W. Van Der Wiede, F.T. Lee Jr. (2007). Microwave ablation with multiple simultaneously powered small gauge triaxial antennas: result from an in vivo swine liver model, Radiology, vol. 244 (1), July 2007, pp. 151-6.

[14] D. Yang, J.M. Bertram, M.C. Converse, A.P. O'Rourke, J.G. Webster, S.C. Hagness, J.A. Will and D.M. Mahvi (2006). A floating sleeve antenna yield localized hepatic microwave ablation, IEEE transactions on Biomedical Engineering, vol. 53 (3), March 2006, pp. 533-7.

[15] P. Prakash, G. Deng, M.C. Converse, J.G. Webster, D.M. Mahvi and M.C. Ferris (2008). Design optimization of a robust sleeve antenna for hepatic microwave ablation, Physics in medicine and Biology, vol. 53 (4), February (2008), pp. 1057-69.

[16] K. Saito, H. Yoshimura, K. Ito, Y. Aoyagi and H. Horita (2004). Clinical trials of interstitial microwave hyperthermia by use coaxial-slot antenna with two slots, IEEE Transactions on Microwave theory and techniques, vol. 52 (8), August 2004, pp. 1987-91.

[17] J.M. Bertram, D. Yang, M.C. Converse, J.G. Webster and D.M. Mahvi (2006). Antenna design for microwave hepatic ablation using an axisymmetric electromagnetic model, Biomedical Engineering Online, vol. 5, February 2006, pp. 1-9.

[18] L. Hadizafar, M.N. Azarmanesh and M. Ojaroudi (2011). Enhance bandwidth double-fed microstrip slot antenna with a pair of L-shaped slots, Progress in Electromagnetics research, vol. 18, November 2010, pp. 47-57

[19] J.M. Bertram, D. Yang, M.C. converse, J.G. Webster and D.M. mahvi (2006). A review of coaxial-based interstitial antennas for hepatic microwave ablation, critical Rev., Biomed. Eng., vol. 34 (3), pp. 187-213.

[20] P. Keangin, P. Rattanadecho and T. Wessapan (2011). An analysis of heat transfer in liver tissue during microwave ablation using single and double slot antenna, International communications in Heat and Mass Transfer, vol. 38 (6), July 2011, pp. 757- 66.

[21] P.E. Clark, R.D. Wooddruff, R.J. Zagoria and M.C. Hall (2007). Microwave ablation of renal parenchymal tumors before nephrectomy: phase I study, American Journal of Roentgenoiogy, vol. 188 (5), May 2007, pp. 1212-4.

[22] P. Phasukkit, S. Tungjitkusolmun and M. Sangworasil (2009). Finite-element analysis and in vitro experiments of placement configurations using triple antennas in microwave hepatic ablation, IEEE Transactions on Biomedical Engineering, vol. 56 (11), November 2009, pp. 2564-72.

[23] M. Li, X.L. Yu, P. Liang, F. Liu, B. Dong and P. Zhou (2012). Percutaneous microwave ablation for liver cancer adjacent to the diaphragm, International Journal of Hyperthermia, vol. 28 (3), pp. 218-26.

[24] I. Obaidat, B. Issa, and Y. Haik (2015). Magnetic properties of magnetic nanoparticles for efficient hyperthermia, Nanomaterial, vol. 6 2015, pp. 63-89.

[25] D.R. Di, Z.Z. He, Z.Q. Sun, J. Liu (2012). A new nano-cryosurgical modality for tumor treatment using biodegradable MgO nanoparticles, Nanomedicine: Nanotechnol., Biol.Med., vol. 8 (8), November 2012, pp. 1233-41.

[26] JF. Yan, J. Liu (2008). Nanocryosurgery and its mechanism for enhancing freezing efficiency of tumor tissues,

Nanomedicine: Nanotechnology, Biology Medicine, vol. 4 (1), March 2008, pp. 79-87.

[27] Y.L. Shao, B. Arjun, H.L. Leo and K.J. Chua (2017). Nano-assisted radiofrequency ablation of clinically extracted irregularly-shaped liver tumors, Journal of Thermal Biology, vol. 66, 2017, pp. 101-13.

[28] A. Nakayama and F. Kuwahara (2008). A general bioheat transfer model based on the theory of porous media, International Journal of Heat and Mass transfer, vol. 51 (11-12), June 2008, pp. 3190-9.

[29] S. Mahajoob and K. Vafai (2009). Analytical characterization of heat transport through biological media incorporating hyperthermia treatment, International Journal of Heat and Mass Transfer, vol. 52 (5-6), February 2009, pp. 1608-18.

[30] P.R. Stauffer, F. Rossetto, M. Prakash, D.G. Neuman and T. Lee (2003). Phantom and animal tissue for modeling the electrical properties of human liver, International Journal of Hyperthermia, vol. 19 (1), January-February 2003, pp. 89-101.

[31] D. Yang, M. Converse, D.M. Mahvi and J.G. Webster (2007). Expanding the bioheat equation to include tissue internal water evaporation during heating, IEEE Transactions on Biomedical Engineering, vol. 54 (8), August 2007, pp. 1382-8.

[32] T. Wessapan, S. Srisawatdhisukul and P. Rattanadecho (2011). The effects of dielectric shield on specific absorption rate and heat transfer in the human body exposed to leakage microwave energy, International Communications in Heat and Mass Transfer, vol. 38 (2), February 2011, pp. 255-62.

[33] P. Rattanadecho, and P. Keangin, (2013). Numerical study of heat transfer and blood flow in two-layered porous liver tissue during microwave ablation process using single and double slot antenna, International Journal of heat and mass Transfer, vol. 58(1-2), March 2013, pp. 457-70.

[34] K.C. Leong, C. Yang, S.M.S Murshed (2006). A model for the thermal conductivity of nanofluids–the effect of interfacial layer. J. Nanopart. Res. vol 8 (2), April 2006, pp. 245-54.

[35] J. Glory, M. Bonetti, M. Helezen, M. Mayne-L Hermite, C. Reynaud (2008). Thermal and Electrical conductivities of water-based nanofluids prepared with long multiwalled carbon nanotubes. J. Appl. Phys. 103 (9), February 2008, pp. 094309(1-7).

[36] I. Obaidat, B. Issa, and Y. Haik (2015). Magnetic properties of magnetic nanoparticles for efficient hyperthermia, Nanomaterial, vol. 6 2015, pp. 63-89.

[37] D.R. Di, Z.Z. He, Z.Q. Sun, J. Liu (2012). A new nano-cryosurgical modality for tumor treatment using biodegradable MgO nanoparticles, Nanomedicine: Nanotechnol., Biol.Med., vol. 8 (8), November 2012, pp. 1233-41.

[38] JF. Yan, J. Liu (2008). Nanocryosurgery and its mechanism for enhancing freezing efficiency of tumor tissues, Nanomedicine: Nanotechnology, Biology Medicine, vol. 4 (1), March 2008, pp. 79-87.

[39] Y.L. Shao, B. Arjun, H.L. Leo and K.J. Chua (2017). Nano-assisted radiofrequency ablation of clinically extracted irregularly-shaped liver tumors, Journal of Thermal Biology, vol. 66, 2017, pp. 101-13.